

Elucidating the structural evolution of a highly porous responsive metal-organic framework (DUT-49(M)) upon guests desorption by time-resolved in-situ powder X-ray diffraction

*Bikash Garai,^a † Volodymyr Bon,^{*a} Francesco Walenszus,^a Azat Khadiev,^b Dmitri Novikov,^b*

*Stefan Kaskel^{*a}*

^aChair of Inorganic Chemistry I, Technische Universität Dresden, Bergstraße 66, 01069, Dresden, Germany

^bP23 Beamline, PETRA III - DESY Photon Science, Notkestraße 85, 22607, Hamburg, Germany

KEYWORDS: flexible MOFs, in situ PXRD, DUT-49, desolvation.

Removal of the guest molecules from the pores of Metal-Organic Frameworks (MOFs) is one of the critical steps in particular for highly porous frameworks associated with high internal stress. In case of isostructural mesoporous DUT-49(M) (M – Cu, Ni, Mn, Fe, Co, Zn, Cd) frameworks, only DUT-49(Cu) and DUT-49(Ni) could be successfully desolvated so far and only by using supercritical activation. To get a deeper insight into the processes occurring upon the desorption of the solvent from the pores of DUT-49(M) the desolvation was monitored in situ by synchrotron PXRD. Analysis of the time-resolved PXRD data shows the full structural pathway of the solid, which involves continuous and discontinuous phase transitions from open pore (op) to

intermediate pore (ip) phase and from ip to contracted pore (cp) phase for DUT-49(Cu) and DUT-49(Ni). For DUT-49(Zn), the op to ip transition is directly followed by amorphization of the framework. All other frameworks show direct amorphization of the op phase.

Introduction

MOFs are 3-dimensional architectures constructed via the coordination of metal ions or cluster as nodes and organic linkers as struts, resulting in crystallographically well defined porosity.¹⁻⁴ After removing the guest molecules from the pores, record values of surface area and pore volumes can be reached.⁵⁻⁷ The application potential of MOFs is ranging from typical for porous materials application such as gas storage,⁸ separation⁹ and catalysis¹⁰ to a rather specific application for crystalline porous solids e.g. sensors¹¹ and electronic devices.^{12, 13}

One of the unique properties of MOFs is stimuli-induced framework switchability, which is reflected in the structural response as an answer of chemical and electrochemical stimuli and associated with the change in porosity and pore accessibility.¹⁴⁻¹⁶ This feature of the flexible framework can be effectively used for enhancing the gas storage capacity¹⁷⁻¹⁹ or gas separation selectivity^{20,21} and particular cases outperform their rigid analogues. Due to their specific mechanic properties, flexible MOFs are also often discussed for applications as shock absorbers or nano springs.^{22,23} Based on the kinetics of the structural transformations of the framework, these porosity changes are termed as gating, breathing, swelling or subnetwork displacement.¹⁵

The gating is usually specified by the threshold activation energy, which must be reached to induce the phase transition. For guest-induced breathing, the threshold chemical potential should be reached to induce the transition from usually dense closed pore phase to porous open pore phases. The archetypical examples of gating are observed in $\text{Cu}(\text{bipy})_2(\text{BF}_4)_2$ also known as ELM-

11²⁴ and Ni₂(ndc)₂dabco, also known as DUT-8(Ni).²⁵ Multi-step gating behaviour upon adsorption of nitrogen at 77 K was observed in Co(bdp) framework.²⁶ The prototypical example of breathing MOF is MIL-53(Al), where two-phase transitions are observed upon adsorption of carbon dioxide in the broad temperature range.^{27, 28} In the first step, the cooperative contraction of the framework from a large pore phase to narrow pore phase is observed upon the adsorption of one CO₂ molecule per unit cell. Further adsorption leads to the reopening of the framework to large pore phase, filled with CO₂ molecules.²⁹

A unique type of breathing has been recently discovered in the hierarchical mesoporous Cu₂(BBCDC) framework, further denoted as DUT-49(Cu).³⁰ The MOF is constructed from the coordination of tetratropic H₄BBCDC linker with Cu-Cu paddlewheel, forming three distinct types of pores: cuboctahedral MOPs with 10 Å in diameter, interconnected by edges *via* biphenyl moieties and form additional tetrahedral (17 Å) and octahedral (24 Å) cages.³¹ The framework can be desolvated by exchange with supercritical CO₂ without losing crystallinity. Adsorption of subcritical fluids at the temperatures close to the standard boiling point trigger the framework contraction from *op* phase to *cp* phase accompanied by the spontaneous gas release phenomenon and pressure increase, called NGA.³⁰ Further increase of the pressure leads to the framework reopening to *op* phase. Desorption of the gas is characterized by the reversible transition to *cp* phase showing the broad hysteresis. NGA transitions originate from the flexibility of the biphenyl spacer of the linker, which undergoes buckling induced by the adsorption stress.³² This directs the framework to undergo a structural transition from a mesoporous *op* phase to a microporous *cp* phase with significantly reduced specific pore volume. Sequential studies have shown the effect of spacer rigidity and variation in adsorption stress.³³ A change in particle size has also been found to impact the NGA response.³⁴ Moreover, host-guest and guest-guest interactions, the influence of

the defects, introduced in a controlled way to the framework was studied by in situ ^{129}Xe NMR.³⁵
³⁶ Most recently, we have studied the role of variation of the metal centres on the flexibility and NGA in the framework.³⁷

Variation in the metal centres of M-M paddle-wheel SBU results in the formation of isostructural DUT-49(M) frameworks. However, the porosity of the framework was found to be different for each of the structures. While a high and moderate porosity was obtained for DUT-49(Cu) and DUT-49(Ni), respectively, other members of the series [DUT-49(M); M= Mn, Fe, Co, Zn, Cd] show very low porosity and shapes of the adsorption isotherms which is not expected for op phases of these MOFs. Investigation on those MOFs revealed that those frameworks undergo structural collapse during the solvent removal at the activation step. Thus, herein, we aimed to study the detailed structural transformations that are possibly occurring during the removal of the subcritical fluid from the framework.

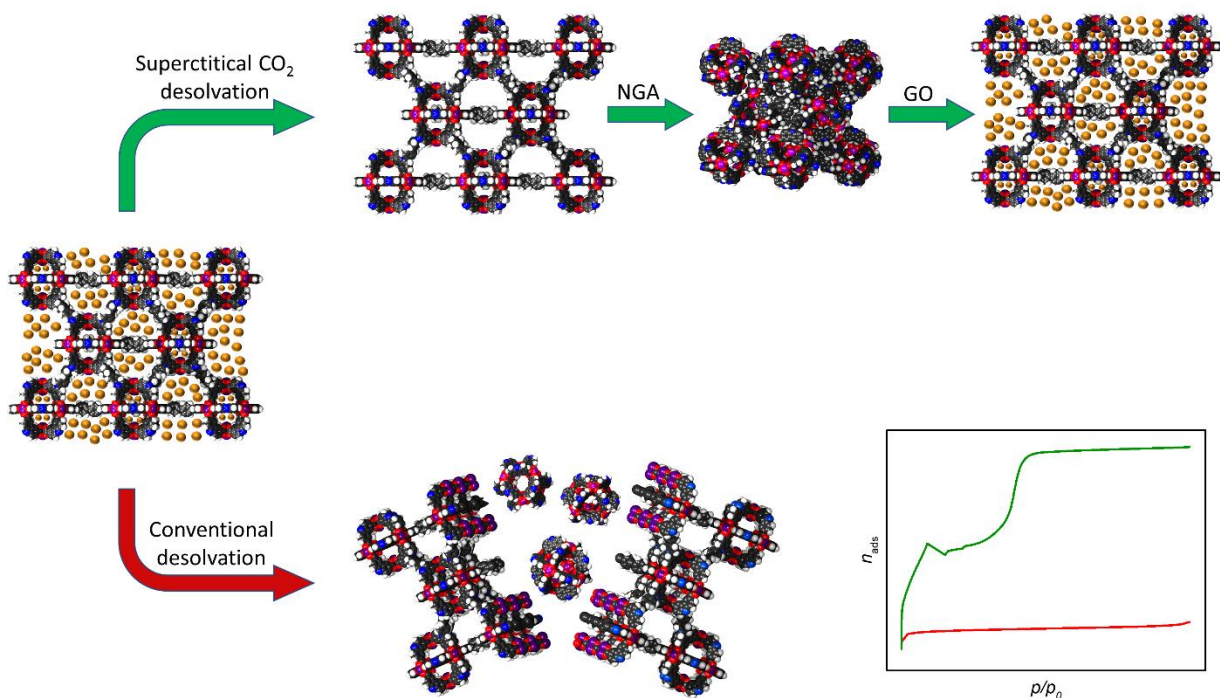


Figure 1. Conventional and supercritical pathways of solvent removal from the DUT-49(Cu) framework, followed by the structural transitions upon adsorption of guests and typical adsorption isotherms.

Removal of solvent during activation of MOFs can be achieved by following approaches: conventional evaporation, freeze-drying and supercritical carbon dioxide activation.³⁸ These methods differ in the amount of internal stress acting on the framework upon removal of the solvent molecules. Direct removal of the solvent in the subcritical state from the MOF pores creates the largest stress. If the mechanical stability of the framework is high enough to sustain the stress, the guest molecules can be removed from the pores in the subcritical state without the framework collapse. Otherwise, the fluid should be transferred to the supercritical state to minimize the intermolecular interactions and therefore reduce the capillary forces upon removal from the pores. Most of the mesoporous MOFs are characterized by a low bulk modulus and supercritical carbon dioxide activation is the only way to remove the guest molecules from the pores. However, in some particular cases, even supercritical activation cannot prevent the framework collapse. DUT-49 is a perfect example for investigation of the guest desorption from the pored because of its hierarchical pore structure, composed of both micro- and mesopores, but also because of the variety of the metal centres, from which only two of them remain crystalline after supercritical drying procedure. Hence, in the following we address two critical questions to achieve a better understanding of framework desolvation and its impact on structure and porosity of frameworks: 1) Why only DUT-49(Cu) and DUT-49(Ni) retain the crystallinity after the supercritical drying procedure and what is the difference to other DUT-49(M) frameworks?; 2) What is the pathway of the structural collapse of the frameworks upon solvent desorption? In order to answer these questions unambiguously, the supercritical CO₂ activation should be followed by PXRD, which is

quite challenging since the cell should be transparent for X-rays, sustain the pressures over 100 bar and temperatures ranging from 283 K to 313 K. Since these conditions are , we monitored the conventional solvent desorption on a series of DUT-49(M) (M – Cu, Ni, Co, Fe, Zn, Mn, Cd) using acetone as a working fluid by time-resolved synchrotron PXRD aiming to access the structural pathways of the framework collapse.

Experimental Section

Synthesis of the ligand and MOFs

The organic linker (H₄BBCDC) was synthesized and characterized using the same procedure as described in the previous report.³¹ Suitably sized single crystals of the MOF were obtained through the post-synthetic metal exchange, starting from DUT-49(Co). DUT-49(Co) was synthesized from the direct solvothermal reaction of H₄BBCDC linker and Co(NO₃)₂·6H₂O in NMP, as block-shaped crystals. The crystals were then washed with fresh NMP to remove the unreacted starting materials and any other impurities. These fresh crystals were then subjected to metal exchange from NMP solvent as per the previously reported pathway, to get single crystals of DUT-49(M) [M = Mn, Fe, Ni, Cu, Zn, Cd] MOFs. These newly obtained MOFs were then washed with fresh NMP until free from any residual metal ion and stored inside fresh NMP. For solvent exchanged MOFs, the NMP soaked MOF crystals were dipped into the respective solvent and then the supernatant liquid was exchanged with fresh solvent for 6 times over a period of 24 h. These crystals were then stored in the same solvent and directly selected for diffraction measurement experiment. The desolvated crystal of DUT-49(Cu) was prepared through supercritical CO₂ treatment to acetone exchanged crystal, using a Jumbo Critical Point Dryer 13200J AB (SPI Supplies). In this process, MOF crystals from dry acetone were taken in a sintered crucible with an aliquot of the solvent and then

placed inside the dryer. Acetone was then exchanged with ultra-pure (99.995 %) liquid carbon dioxide at 17 °C for 10 times over a period of 5 days. The temperature and pressure inside the dryer compartment were then raised above the critical point of carbon dioxide and the samples were left in this supercritical fluid for around 15 min. The pressure was then reduced through the slow release of the fluid over 3 h. The chamber was then flushed with Ar for 15 min and then immediately transferred into an Ar-filled glove box.

Materials and Methods

PXRD patterns of as made DUT-49(M) powders were obtained at room temperature on STOE STADI P diffractometer using Cu-K α 1 radiation ($\lambda = 1.54059 \text{ \AA}$) and a 2D detector (Mythen, DECTRIS). All measurements were performed in transmission geometry using a rotating flatbed sample holder, 2θ steps of 0.015° and exposition time of 20 s per step.

Time-resolved in situ PXRD during the framework desolvation

Time-resolved in situ PXRD experiments were performed at P23 beamline of PETRA III synchrotron, operated by DESY (Hamburg, Germany). The powder of DUT-49(M) in acetone solution was fixed in a borosilicate capillary ($d = 0.5 \text{ mm}$). The capillary was inserted in a specially designed capillary holder, centred in the synchrotron beam. The capillary was connected to the gas flow setup by 1/8" ultra-torr connector from Swagelok®. The setup is controlled by MFC, allowed to align the nitrogen flow in the range of 0.1 – 100 ml/hour. Pure nitrogen (99.99 %) purity was used in experiments (Fig. S2, ESI). Monochromatic radiation with $E = 18.7 \text{ keV}$ ($\lambda = 0.663 \text{ \AA}$) was used in all experiments. PXRD patterns were measured with 1 s. intervals in transmission geometry using PILATUS 1M detector. Silicon powder was used as an external standard for calibration of the system. DAWN software was used for integration of the diffraction images.³⁹ The flow rates

of 5 ml/min and 2 ml/min were used in experiments. Le Bail fit of the selected patterns was performed using FullProf.⁴⁰

Time-resolved optical microscopy

The video recordings were conducted using an Olympus IX70 inverted microscope. The microscope was equipped with a Sony Alpha 6000 camera. Using a 20x objective and an additional 1.5x objective, the magnification was increased to 30x. To determine the crystal size, the pixels of the camera were first calibrated using different grids. To determine the edge length of the crystal, a frame at the beginning of the sequence and a frame at the end was saved individually. From these images the dimensions were determined using the Software ImageJ version 1.51f. The crystal was measured in height and width and the average value was set as edge length. Since the crystals are cubic, this simplification is valid. The cubic DUT-49(Cu) crystal was placed in dimethylformamide on a microscope slide. Afterwards, a video with an original length of 21.41 min was recorded and the contraction of the crystal while ambient pressure solvent evaporation was studied. The resulting video was cut to the relevant part for better clarity. The video was cropped, and the speed was increased by a factor of 10.

Results and Discussion

All materials were synthesized as described previously. DUT-49(Co) was obtained via solvothermal reaction and DUT-49(M) frameworks were obtained using a post-synthetic metal exchange procedure. The phase purity and crystallinity of the frameworks was confirmed by PXRD (see ESI, Fig. S1). Further, the guest molecules in the pores were exchanged from NMP to

acetone to increase the desorption rate. To answer the above-posted questions, we followed desorption of acetone from MOF pores in-situ using time-resolved powder X-ray diffraction at P23 beamline of PETRA-III synchrotron, operated at DESY.

For the case of all DUT-49(M) MOFs, the initial crystalline pattern was in good agreement with that of the respective calculated pattern (Fig. S1, ESI). The first and most intensive peak in the pattern at $2\theta = 1.411^\circ$ corresponds to the (111) lattice plane and is, therefore, suitable for the monitoring of the phase transition. It is noteworthy that during the adsorption or desorption induced transition in DUT-49(Cu), this peak shifted to higher 2θ angles as a result of the isotropic two-fold unit cell contraction, accompanied by lowering of symmetry from $Fm\bar{3}m$ to $Pa\bar{3}$. Since acetone is a subcritical fluid at experimental conditions, the same pathway as previously observed upon desorption of methane (111K) or *n*-butane (273K) is expected.

Indeed, desorption of acetone from DUT-49(Cu) at 298 K shows similar two-step phase transition: 1) shift of the 111 peak to 1.51° indicates the formation of *ip* phase with $a = 43.58 \text{ \AA}$; 2) shift of 111 reflection to 1.82° , which corresponds to the *cp* phase of the MOF with $a = 36.16 \text{ \AA}$ (Fig.2a). This phase is observed only in one PXRD pattern (1 s) showing further complete loss of crystallinity and indicating the structural collapse of the framework, as typically observed upon conventional activation of DUT-49. The change is accompanied by a characteristic colour change from blue to green.

To evaluate the macroscopic changes of the material during the desorption, the time-resolved study of desorption of the DMF from DUT-49(Cu) was monitored by optical microscopy (supplementary video). Initially, the dark cloudy regions and cracks appear on the four corners of the cube simultaneously, accompanied by the shrinkage of the crystal. In terms of the crystal size,

the initial size of the crystal edge was determined as 94.8 μm . For a perfectly cubic crystal, this corresponds to a crystal volume of 851971 μm^3 . After the structural transition, the resulting crystal has an edge length of 68.2 μm which results in a crystal volume of 317214 μm^3 . Based on these values, the crystal volume reduces by 63 % from its initial size. This value is 10% higher in comparison to the value, calculated from *op* and *cp* structures.³⁰ However, in situ PXRD data suggest rapid decomposition of the *cp* phase to the more dense amorphous phase.

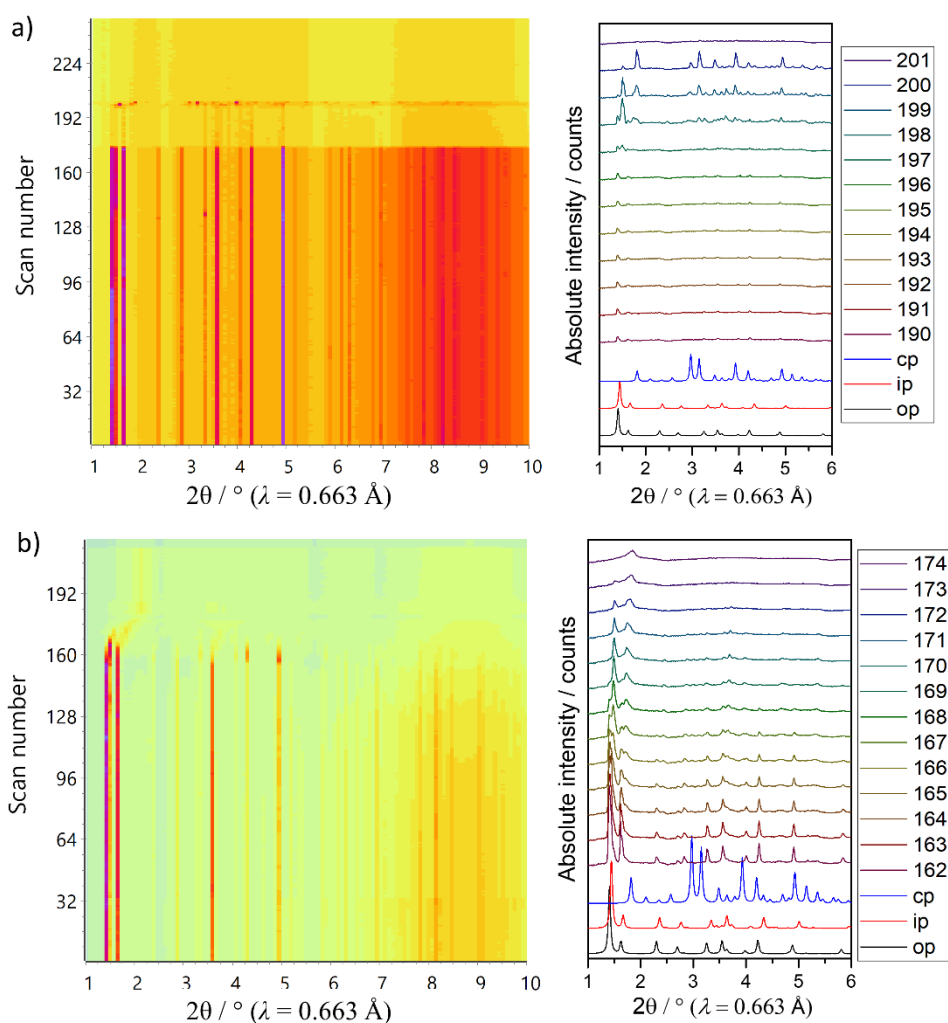


Figure 2. Time-resolved synchrotron PXRD upon desorption of acetone from the pores of (a) DUT-49(Cu) and (b) DUT-49(Ni).

In the next step, we performed in situ desorption of acetone from the pores of DUT-49(Ni), the second MOF from the series, which can be desolvated by supercritical CO₂. Time-resolved PXRD measurements on DUT-49(Ni) under nitrogen flow show a similar trend as observed for DUT-49(Cu) (Fig.2b). Analysis of individual PXRD patterns in the range of transition shows the splitting of 111 peak indicating the phase coexistence in the patterns (165-168). Further desorption leads to the formation of the cp phase, confirmed by the appearance of the reflection at $2\theta=1.84^\circ$.

In further experiments, we subjected DUT-49(M) (M – Fe, Co, Zn, Cd) to time-resolved PXRD experiments using the same nitrogen flow (Fig.3).

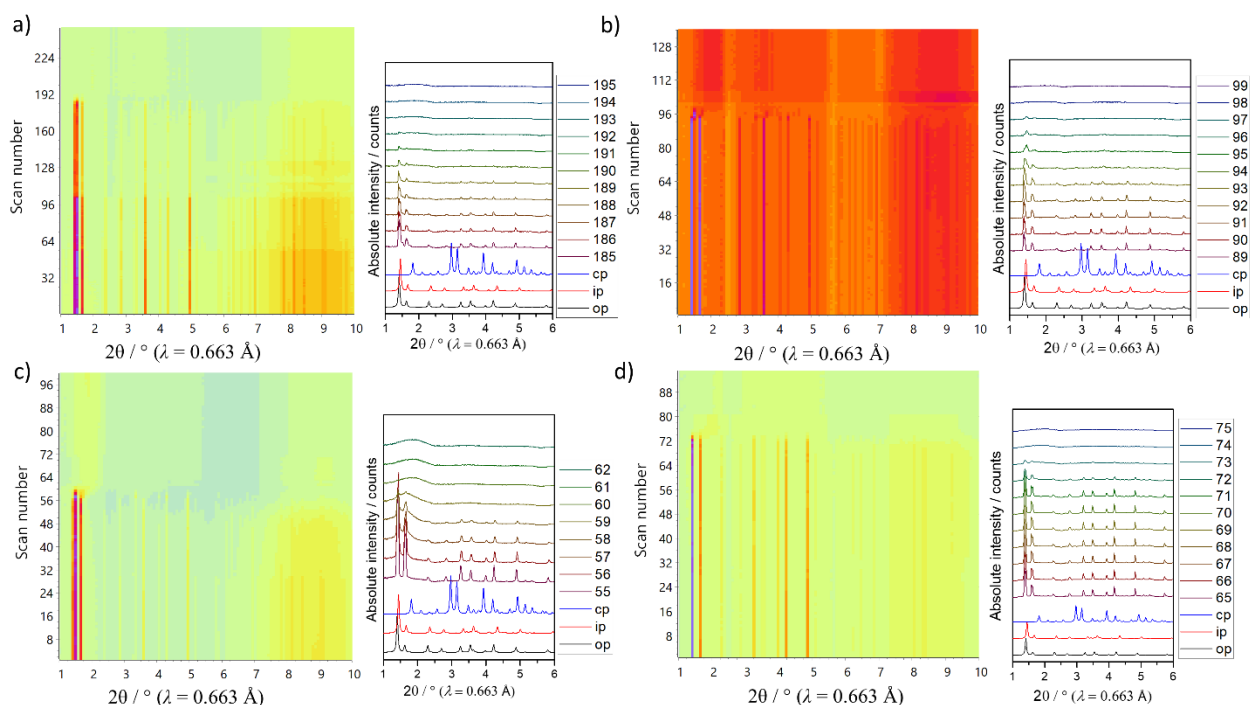


Figure 3. Time-resolved synchrotron PXRD upon desorption of acetone from the pores of (a) DUT-49(Co), (b) DUT-49(Zn), (c) DUT-49(Fe) and (d) DUT-49(Cd).

In the cases of DUT-49(Co), DUT-49(Fe) and DUT-49(Cd), completely different behaviour was observed upon solvent desorption. In all these cases, no shifts in the positions of the reflection

were observed. The intensity of 111 reflection, belonging to the *op* phase vanished at some point indicating the loss of the 3D ordering of the structures. Interestingly, in case of DUT-49(Zn) the formation of the intermediate phase could be proven by the shift of 111 reflection from $2\theta = 1.39^\circ$ to $2\theta = 1.46^\circ$ (Fig.3b).

These results exactly reflect the behaviour of DUT-49(M) solids in the desolvation and in case of DUT-49(Ni) and DUT-49(Cu) exactly followed the pathway of the structural transitions earlier observed in the gas desorption experiments, namely moving along the free energy landscape and reaching the second minima, which is reflected in the *cp* phase. Interestingly, the *cp* phase could be observed only in few PXRDs, namely in the time frame of few seconds, shortly before the framework loses the ordering. Interestingly, this observation contradicts to *in situ* PXRD data measured upon desorption of methane at 111K and other gases, indicating the integrity of *cp* phase even after complete desorption of the fluid. Refinement of the profile for the patterns close to the transition shows no changes in the unit cell in DUT-49(Cd), DUT-49(Fe) and DUT-49(Co) until amorphization (Fig. 4). In the case of DUT-49(Zn), an *op* to *ip* transition could be observed before amorphization, however, no *cp* phase was detected. For DUT-49(Ni), the full pathway *op* \rightarrow *ip* \rightarrow *cp* could be followed. Due to the low signal-to-noise ratio, the profile data on DUT-49(Cu) could not be analyzed quantitatively.

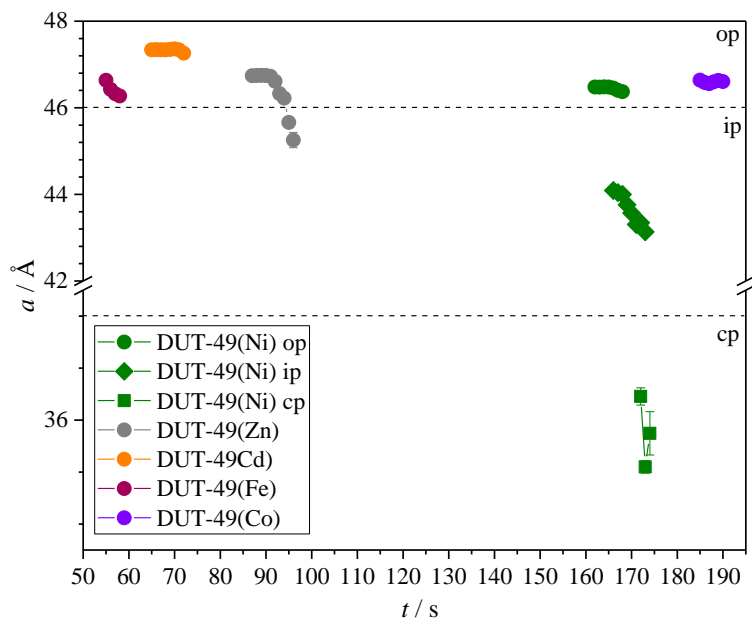


Figure 4. Evolution of the unit cell parameters of DUT-49(M) with time upon desorption of acetone (only PXRDs measured directly before contraction were analyzed).

In case of DUT-49(M) (M - Co, Fe, Mn, Cd), a gradual loss in crystallinity was observed upon desorption of acetone from the pores. Taking into account the fact that all frameworks are isostructural and the same guests and experimental conditions were used in all experiments the metal centre plays a crucial role in reducing the mechanical stability of entire frameworks controlling the response on internal stress. In situ experiments can be also considered as direct proof of the bistability of the framework, which could be confirmed only for DUT-49(Cu) and DUT-49(Ni). Interestingly, DUT-49(Zn) shows the stable *ip* phase, which loses crystallinity upon further desorption of the guests. Although the constant gas flow and identical capillaries were used in all above experiments, the absolute stability cannot be directly extracted from the data because of the different powder packing and position of the capillary in the beam. As an example, for DUT-49(Cu) we studied the influence of the gas flow rate on the pathway of the crystal structure,

however, even reducing of the gas flow rate from 5 ml/min to 2 ml/min, indicates no formation of additional phases upon desorption of acetone (Fig. 2a).

Conclusions

Summarizing, we studied the desolvation mechanism in DUT-49(M) (M – Mn, Fe, Co, Ni, Cu, Zn, Cd) frameworks by time-resolved in situ synchrotron PXRD. Desolvation of DUT-49(Cu) and DUT-49(Ni), which retain their structures after supercritical activation and show adsorption induced flexibility, follow a similar pathway, as observed in desorption experiments. For these cases an $op \rightarrow ip$ transition, triggered by elastic deformation of the ligand, is followed by an $ip \rightarrow \epsilon p$ transition, caused by inelastic buckling of the linker. The cp phase loses crystallinity within few seconds, which differs from the observations made by *in situ* PXRD studies upon adsorption/desorption of methane at 111 K. DUT-49(Zn) shows the continuous $op \rightarrow ip$ transition, but hereafter loss of crystallinity, which is an indicator of the absence of the bistability, required for flexibility and NGA. The op phases of DUT-49(M) (M – Mn, Fe, Co, Cd) show direct amorphization without any signs of phase transitions, attributed by the low stability of the corresponding paddle-wheels. Although *in silico* calculations can predict the free energy profile in some particular cases, experimental monitoring of the MOF desolvation can be considered as a valuable technique for estimating bistability in MOFs. Besides, a detailed analysis of PXRD patterns by profile matching and even Rietveld refinement could provide meaningful information for the development of adsorption/desorption driven stress models for MOFs.

ASSOCIATED CONTENT

Supporting Information. The following files are available free of charge. Electronic supporting information (PDF), supporting video.

AUTHOR INFORMATION

Corresponding Author

*Correspondence should be addressed to volodymyr.bon@tu-dresden.de and stefan.kaskel@tu-dresden.de

Present Addresses

†New York University Abu Dhabi.

Author Contributions

B.G. performed synthesis and characterization of organic ligand, MOFs, post-synthetic metalation and solvent exchange. B.G., V.B., A.K., and D.N. designed and performed time-resolved *in situ* PXRD experiments. F.W. conducted in situ desorption experiment on DUT-49(Cu) single crystal using an optical microscope. B.G., V.B. and S.K. wrote the manuscript. V.B. and S.K. coordinated the project.

Funding Sources

This project has received funding from the European Research Council (ERC) under the European Union's Horizon 2020 research and innovation programme (grant agreement No. 742743). V.B. thanks the BMBF (Project No. 05K19OD2) for financial support.

ACKNOWLEDGMENT

The authors thank PETRA III (DESY) for the allocation of the synchrotron radiation beamtime on P23 beamline (Proposal I-20181184) and travel grants.

ABBREVIATIONS

MOF, Metal-Organic Framework; ELM; Elastic Layered Material; DUT, Dresden University of Technology; MIL, Materials Institut Lavoisier; MOP, Metal-Organic Polyhedron; H₄BBCDC, 9,9' -([1,1' -biphenyl]-4,4' -diyl)-bis(9H-carbazole-3,6-dicarboxylic acid); NGA, Negative Gas Adsorption; PXRD, Powder X-Ray Diffraction; NMP, *N*-Methyl-2-pyrrolidone; DESY, Deutsche Elektronen Synchrotron; *op*, open pore; *ip*, intermediate pore; *cp*, contracted pore.

REFERENCES

- (1) Kitagawa, S.; Kitaura, R.; Noro, S.-i., Functional Porous Coordination Polymers. *Angew. Chem., Int. Ed.* **2004**, 43, (18), 2334-2375.
- (2) Eddaoudi, M.; Moler, D. B.; Li, H.; Chen, B.; Reineke, T. M.; O'Keeffe, M.; Yaghi, O. M., Modular Chemistry: Secondary Building Units as a Basis for the Design of Highly Porous and Robust Metal–Organic Carboxylate Frameworks. *Acc. Chem. Res.* **2001**, 34, (4), 319-330.
- (3) Batten, S. R.; Champness, N. R.; Chen, X.-M.; Garcia-Martinez, J.; Kitagawa, S.; Öhrström, L.; O'Keeffe, M.; Suh, M. P.; Reedijk, J., Coordination polymers, metal–organic frameworks and the need for terminology guidelines. *CrystEngComm* **2012**, 14, (9), 3001-3004.
- (4) Furukawa, H.; Ko, N.; Go, Y. B.; Aratani, N.; Choi, S. B.; Choi, E.; Yazaydin, A. Ö.; Snurr, R. Q.; O'Keeffe, M.; Kim, J.; Yaghi, O. M., Ultrahigh Porosity in Metal-Organic Frameworks. *Science* **2010**, 329, (5990), 424.
- (5) Hönicke, I. M.; Senkovska, I.; Bon, V.; Baburin, I. A.; Bönisch, N.; Raschke, S.; Evans, J. D.; Kaskel, S., Balancing Mechanical Stability and Ultrahigh Porosity in Crystalline Framework Materials. *Angew. Chem., Int. Ed.* **2018**, 57, (42), 13780-13783.
- (6) Farha, O. K.; Eryazici, I.; Jeong, N. C.; Hauser, B. G.; Wilmer, C. E.; Sarjeant, A. A.; Snurr, R. Q.; Nguyen, S. T.; Yazaydin, A. Ö.; Hupp, J. T., Metal–Organic Framework Materials with Ultrahigh Surface Areas: Is the Sky the Limit? *J. Am. Chem. Soc.* **2012**, 134, (36), 15016-15021.
- (7) Chen, Z.; Li, P.; Anderson, R.; Wang, X.; Zhang, X.; Robison, L.; Redfern, L. R.; Moribe, S.; Islamoglu, T.; Gómez-Gualdrón, D. A.; Yildirim, T.; Stoddart, J. F.; Farha, O. K., Balancing volumetric and gravimetric uptake in highly porous materials for clean energy. *Science* **2020**, 368, (6488), 297.
- (8) Mason, J. A.; Veenstra, M.; Long, J. R., Evaluating metal–organic frameworks for natural gas storage. *Chem. Sci.* **2014**, 5, (1), 32-51.
- (9) Kang, Z.; Fan, L.; Sun, D., Recent advances and challenges of metal–organic framework membranes for gas separation. *J. Mater. Chem. A* **2017**, 5, (21), 10073-10091.

- (10) Dhakshinamoorthy, A.; Li, Z.; Garcia, H., Catalysis and photocatalysis by metal organic frameworks. *Chem. Soc. Rev.* **2018**, 47, (22), 8134-8172.
- (11) Zhang, Y.; Yuan, S.; Day, G.; Wang, X.; Yang, X.; Zhou, H.-C., Luminescent sensors based on metal-organic frameworks. *Coord. Chem. Rev.* **2018**, 354, 28-45.
- (12) Zhou, H.-C. J.; Kitagawa, S., Metal–Organic Frameworks (MOFs). *Chem. Soc. Rev.* **2014**, 43, (16), 5415-5418.
- (13) Krishtab, M.; Stassen, I.; Stassin, T.; Cruz, A. J.; Okudur, O. O.; Armini, S.; Wilson, C.; De Gendt, S.; Ameloot, R., Vapor-deposited zeolitic imidazolate frameworks as gap-filling ultra-low-k dielectrics. *Nat. Commun.* **2019**, 10, (1), 3729.
- (14) Horike, S.; Shimomura, S.; Kitagawa, S., Soft porous crystals. *Nat. Chem.* **2009**, 1, (9), 695-704.
- (15) Schneemann, A.; Bon, V.; Schwedler, I.; Senkovska, I.; Kaskel, S.; Fischer, R. A., Flexible metal–organic frameworks. *Chem. Soc. Rev.* **2014**, 43, (16), 6062-6096.
- (16) Chang, Z.; Yang, D.-H.; Xu, J.; Hu, T.-L.; Bu, X.-H., Flexible Metal–Organic Frameworks: Recent Advances and Potential Applications. *Adv. Mater.* **2015**, 27, (36), 5432-5441.
- (17) Mason, J. A.; Oktawiec, J.; Taylor, M. K.; Hudson, M. R.; Rodriguez, J.; Bachman, J. E.; Gonzalez, M. I.; Cervellino, A.; Guagliardi, A.; Brown, C. M.; Llewellyn, P. L.; Masciocchi, N.; Long, J. R., Methane storage in flexible metal–organic frameworks with intrinsic thermal management. *Nature* **2015**, 527, (7578), 357-361.
- (18) Kundu, T.; Shah, B. B.; Bolinois, L.; Zhao, D., Functionalization-Induced Breathing Control in Metal–Organic Frameworks for Methane Storage with High Deliverable Capacity. *Chem. Mater.* **2019**, 31, (8), 2842-2847.
- (19) Kundu, T.; Wahiduzzaman, M.; Shah, B. B.; Maurin, G.; Zhao, D., Solvent-Induced Control over Breathing Behavior in Flexible Metal–Organic Frameworks for Natural-Gas Delivery. *Angew. Chem., Int. Ed.* **2019**, 58, (24), 8073-8077.
- (20) Sato, H.; Kosaka, W.; Matsuda, R.; Hori, A.; Hijikata, Y.; Belosludov, R. V.; Sakaki, S.; Takata, M.; Kitagawa, S., Self-Accelerating CO Sorption in a Soft Nanoporous Crystal. *Science* **2014**, 343, (6167), 167.
- (21) Taylor, M. K.; Runčevski, T.; Oktawiec, J.; Bachman, J. E.; Siegelman, R. L.; Jiang, H.; Mason, J. A.; Tarver, J. D.; Long, J. R., Near-Perfect CO₂/CH₄ Selectivity Achieved through Reversible Guest Templating in the Flexible Metal–Organic Framework Co(bdp). *J. Am. Chem. Soc.* **2018**, 140, (32), 10324-10331.
- (22) Krause, S.; Evans, J. D.; Bon, V.; Senkovska, I.; Ehrling, S.; Stoeck, U.; Yot, P. G.; Iacomi, P.; Llewellyn, P.; Maurin, G.; Coudert, F.-X.; Kaskel, S., Adsorption Contraction Mechanics: Understanding Breathing Energetics in Isorecticular Metal–Organic Frameworks. *J. Phys. Chem. C* **2018**, 122, (33), 19171-19179.
- (23) Yot, P. G.; Boudene, Z.; Macia, J.; Granier, D.; Vanduyfhuys, L.; Verstraelen, T.; Van Speybroeck, V.; Devic, T.; Serre, C.; Férey, G.; Stock, N.; Maurin, G., Metal–organic frameworks as potential shock absorbers: the case of the highly flexible MIL-53(Al). *Chem. Commun.* **2014**, 50, (67), 9462-9464.
- (24) Hiraide, S.; Tanaka, H.; Miyahara, M. T., Understanding gate adsorption behaviour of CO₂ on elastic layer-structured metal–organic framework-11. *Dalton Trans.* **2016**, 45, (10), 4193-4202.
- (25) Bon, V.; Klein, N.; Senkovska, I.; Heerwig, A.; Getzschmann, J.; Wallacher, D.; Zizak, I.; Brzhezinskaya, M.; Mueller, U.; Kaskel, S., Exceptional adsorption-induced cluster and

- network deformation in the flexible metal–organic framework DUT-8(Ni) observed by in situ X-ray diffraction and EXAFS. *Phys. Chem. Chem. Phys.* **2015**, *17*, (26), 17471-17479.
- (26) Salles, F.; Maurin, G.; Serre, C.; Llewellyn, P. L.; Knöfel, C.; Choi, H. J.; Filinchuk, Y.; Oliviero, L.; Vimont, A.; Long, J. R.; Férey, G., Multistep N₂ Breathing in the Metal–Organic Framework Co(1,4-benzenedipyrzolate). *J. Am. Chem. Soc.* **2010**, *132*, (39), 13782-13788.
- (27) Serre, C.; Millange, F.; Thouvenot, C.; Noguès, M.; Marsolier, G.; Louër, D.; Férey, G., Very Large Breathing Effect in the First Nanoporous Chromium(III)-Based Solids: MIL-53 or CrIII(OH)·{O₂C–C₆H₄–CO₂}·{HO₂C–C₆H₄–CO₂H}_x·H₂O_y. *J. Am. Chem. Soc.* **2002**, *124*, (45), 13519-13526.
- (28) Bourrelly, S.; Llewellyn, P. L.; Serre, C.; Millange, F.; Loiseau, T.; Férey, G., Different Adsorption Behaviors of Methane and Carbon Dioxide in the Isotypic Nanoporous Metal Terephthalates MIL-53 and MIL-47. *J. Am. Chem. Soc.* **2005**, *127*, (39), 13519-13521.
- (29) Serre, C.; Bourrelly, S.; Vimont, A.; Ramsahye, N. A.; Maurin, G.; Llewellyn, P. L.; Daturi, M.; Filinchuk, Y.; Leynaud, O.; Barnes, P.; Férey, G., An Explanation for the Very Large Breathing Effect of a Metal–Organic Framework during CO₂ Adsorption. *Adv. Mater.* **2007**, *19*, (17), 2246-2251.
- (30) Krause, S.; Bon, V.; Senkovska, I.; Stoeck, U.; Wallacher, D.; Többs, D. M.; Zander, S.; Pillai, R. S.; Maurin, G.; Coudert, F.-X.; Kaskel, S., A pressure-amplifying framework material with negative gas adsorption transitions. *Nature* **2016**, *532*, (7599), 348-352.
- (31) Stoeck, U.; Krause, S.; Bon, V.; Senkovska, I.; Kaskel, S., A highly porous metal–organic framework, constructed from a cuboctahedral super-molecular building block, with exceptionally high methane uptake. *Chem. Commun.* **2012**, *48*, (88), 10841-10843.
- (32) Evans, J. D.; Bocquet, L.; Coudert, F.-X., Origins of Negative Gas Adsorption. *Chem* **2016**, *1*, (6), 873-886.
- (33) Krause, S.; Evans, J. D.; Bon, V.; Senkovska, I.; Iacomi, P.; Kolbe, F.; Ehrling, S.; Troschke, E.; Getzschmann, J.; Többs, D. M.; Franz, A.; Wallacher, D.; Yot, P. G.; Maurin, G.; Brunner, E.; Llewellyn, P. L.; Coudert, F.-X.; Kaskel, S., Towards general network architecture design criteria for negative gas adsorption transitions in ultraporous frameworks. *Nat. Commun.* **2019**, *10*, (1), 3632.
- (34) Krause, S.; Bon, V.; Senkovska, I.; Többs, D. M.; Wallacher, D.; Pillai, R. S.; Maurin, G.; Kaskel, S., The effect of crystallite size on pressure amplification in switchable porous solids. *Nat. Commun.* **2018**, *9*, (1), 1573.
- (35) Kolbe, F.; Krause, S.; Bon, V.; Senkovska, I.; Kaskel, S.; Brunner, E., High-Pressure in Situ ¹²⁹Xe NMR Spectroscopy: Insights into Switching Mechanisms of Flexible Metal–Organic Frameworks Isorecticular to DUT-49. *Chem. Mater.* **2019**, *31*, (16), 6193-6201.
- (36) Krause, S.; Reuter, F. S.; Ehrling, S.; Bon, V.; Senkovska, I.; Kaskel, S.; Brunner, E., Impact of Defects and Crystal Size on Negative Gas Adsorption in DUT-49 Analyzed by In Situ ¹²⁹Xe NMR Spectroscopy. *Chem. Mater.* **2020**, *32*, (11), 4641-4650.
- (37) Garai, B.; Bon, V.; Krause, S.; Schwotzer, F.; Gerlach, M.; Senkovska, I.; Kaskel, S., Tunable Flexibility and Porosity of the Metal–Organic Framework DUT-49 through Postsynthetic Metal Exchange. *Chem. Mater.* **2020**, *32*, (2), 889-896.
- (38) Mondloch, J. E.; Karagiari, O.; Farha, O. K.; Hupp, J. T., Activation of metal–organic framework materials. *CrystEngComm* **2013**, *15*, (45), 9258-9264.
- (39) Filik, J.; Ashton, A. W.; Chang, P. C. Y.; Chater, P. A.; Day, S. J.; Drakopoulos, M.; Gerring, M. W.; Hart, M. L.; Magdysyuk, O. V.; Michalik, S.; Smith, A.; Tang, C. C.; Terrill, N.

J.; Wharmby, M. T.; Wilhelm, H., Processing two-dimensional X-ray diffraction and small-angle scattering data in DAWN 2. *J. Appl. Crystallogr.* **2017**, 50, (3), 959-966.

(40) Rodríguez-Carvajal, J., Recent advances in magnetic structure determination by neutron powder diffraction. *Phys. B* **1993**, 192, (1), 55-69.

Graphical abstract

